



Contents lists available at ScienceDirect

Journal of Materials Processing Tech.

journal homepage: [www.elsevier.com/locate/jmatprotec](http://www.elsevier.com/locate/jmatprotec)

## Loop travel-path of fibre laser welded Alclad AA2219-O alloy



Olatunji Oladimeji Ojo<sup>a,b,\*</sup>, Emel Taban<sup>b,c</sup>, Erdinc Kaluc<sup>b,c</sup>

<sup>a</sup> The Federal University of Technology Akure, Ondo State, Nigeria

<sup>b</sup> Kocaeli University, Kocaeli, Izmit, Turkey

<sup>c</sup> Welding Research Education and Training Centre, Kocaeli University, Izmit, Turkey

### ARTICLE INFO

#### Keywords:

Fibre laser welding  
Aluminum alloy  
Mechanical properties  
Weld microstructure  
Weld fracture

### ABSTRACT

A loop or circular travel-path of fibre laser beam on Alclad AA2219-O aluminum alloy plates was investigated by varying laser penetration depths (partial and deep penetrations). Lap joint configuration was employed for the welding process. The mechanical properties and microstructures of the resultant welds were examined. The fracture morphologies of the welds subjected to axial loading were critically examined via scanning electron microscope (SEM). The result shows that loop or circular beam travel-path improves the lap shear failure load of full penetrated welds. The presence of Alclad on the surface of the alloy and penetration depth influence porosity formation in all welds. The fusion regions of welds are predominantly composed of equiaxed grain structures. The returning laser beam reduces the hardness of the start/end (S/E) fusion region and increases porosity level of the region as compared to the travel-path (TP) fusion region. Macro-pores (351–575  $\mu\text{m}$ ) significantly influence fracture pattern of welds whereas micro-pores (50–200  $\mu\text{m}$ ) show no obvious influence on the examined fracture surfaces. The fracture morphologies of partial and full penetrated welds are interfacial ductile shearing/fracture (across the adjoining fusion width) and porosity induced fracture (emanating from the start/end fusion region) respectively.

### 1. Introduction

A few laser beam modifications have been examined on aluminum alloys. Wang et al. (2016) investigated the effect of beam oscillating patterns (transversal, longitudinal and circular) on laser beam welded AA6061-T6 alloy in butt configuration. It was revealed that the formation of equiaxed grain in the fusion zone was generally promoted by beam oscillation. The welds obtained under circular oscillation produced the soundest weld, the finest grain and the largest amount of equiaxed grains. Beam oscillation was reported to have no significant effects on tensile strength, but it increased weld ductility. Enz et al. (2016) examined the effect of an initial large beam diameter, a top-hat beam profile and a high laser power of Yb fibre laser (derived approach of welding) on high-alloyed Al-Zn-Mg-Cu alloys during deep penetration welding. An ideal distribution of irradiance is provided by the top-hat beam profile in such a manner that the laser beam diameter is almost equivalent to the keyhole diameter. This is said to facilitate the realization of large and stable keyhole during the welding process. It was affirmed that porosity and excess penetration deteriorated the weldability of the alloy with increasing Zn + Mg + Cu content while the derived approach of welding improved laser weldability.

Hajavifard et al. (2016) investigated the feasibility of using laser for

spot welding in joining 1100 aluminum alloy by shaping of the laser pulse. Standard pulse shaping, ramp-down pulse shaping and ramp-down with rectangle initial coupling were employed in investigating the spot welding process. It was observed that ramp-down pulse shaping achieved the deepest penetration and weld quality. To reduce manufacturing effort in T-joint welding, double-sided laser beam welding needs to be jettisoned for a more direct and convenient welding approach such as single-sided laser welding. Nevertheless, the occurrence of weld defects in this approach is a major setback which needs to be overcome. Enz et al. (2015) examined single sided beam welding of skin-stringer joints of dissimilar aluminum alloys by using high-power fibre laser with a large/enlarged beam diameter. Improved degassing condition due to the enlarged keyhole in this approach of welding and reduced heat input and penetration into the skin material are responsible for the improved joint efficiency as compared to that of double sided welded joints.

The instances of modifying laser travel-path to improve weld quality are areas that have not been thoroughly expounded in literature. Diverse weld geometries such as T-joints and butt joints have been investigated via the use of laser beam welding method, but the impact of beam travel-path on welds is still short of critical assessment. The travel-path of laser beam on AA2219-O aluminum alloy is modified

\* Corresponding author at: The Federal University of Technology Akure, Ondo State, Nigeria.  
E-mail address: [ojooladimeji90@yahoo.com](mailto:ojooladimeji90@yahoo.com) (O.O. Ojo).

**Table 1**  
Chemical composition of the workpiece in wt.% (Oladimeji et al., 2016).

Alloy	Al	Si	Fe	Cu	Mn	Mg	Cr	Zn	Ti	V	Zr	Others
2219-O	Bal	0.06	0.14	6.6	0.32	0.02	0.00	0.03	0.04	0.06	0.13	0.03

from the well-known single spot or single line keyhole welding to a loop or circular welding path. This approach of welding is adopted because of its propensity to produce welds with longer bonded width/weld area and consequently improved weld quality. Partial and deep penetrations of laser beam on AA2219-O alloy are studied via circular beam travel-path approach. Mechanical and microstructural properties of welds together with the fracture morphologies of welds under axial loading condition are also investigated.

## 2. Material and methods

The workpiece material employed for this research is an Alclad AA2219-O rolled sheet with a thickness of 1.6 mm while the thickness of the surface oxide on the alloy is about 77.36  $\mu\text{m}$ . The compositions of the alloy are given in Table 1 and the alloy's ultimate tensile and yield strengths are 146 MPa and 63 MPa respectively. Internal 2-way beam switch installed fibre laser process was employed in joining the workpieces positioned in overlapped geometry at operating ambient temperature. The optical characteristics of the fibre laser are given in Table 2. The dimensions of the lap shear specimen and the welding beam's travel-path are illustrated in Fig. 1. A loop or circular beam travel-path having a diameter of 12 mm around the center of the overlapped region was employed in joining the work pieces as indicated in Fig. 1. Partial penetration and full penetration of the laser beam into the lower plate were employed for the joining process. A welding speed of 33 mm/s was employed for the entire joining process in order to eliminate the effect of welding speeds on effective fusion width of welds and preliminary experiment was carried out by varying laser power. Two levels of laser power, 3600 W and 3750 W, were employed for the purpose of this report. The incident angle of the laser beam to the workpiece was set at 15° to prevent optical feedback and the distance between the laser head and the workpiece was set as 225 mm for all welds. Samples of the resultant full and partial penetrated welds are shown in Figs. 2 and 3 respectively.

According to TS EN ISO 6892-1 standard, the lap shear failure loads of the resultant weld specimens were obtained by using a computer-controlled tensile machine. A displacement rate of 10 mm/min was employed for all lap shear specimens and the average of three weld samples obtained at the same parameter level was taken as the actual weld strength (lap shear failure load) in all weld categories. The fracture surfaces of welds subjected to axial loading were examined by using secondary electron imaging mode in a JEOL scanning electron microscope (SEM) in order to understand the welds' failure modes. The cross-sectioned weld specimens were mounted in epoxy resin, grounded and polished in electropolishing unit to mirror like outlooks. The

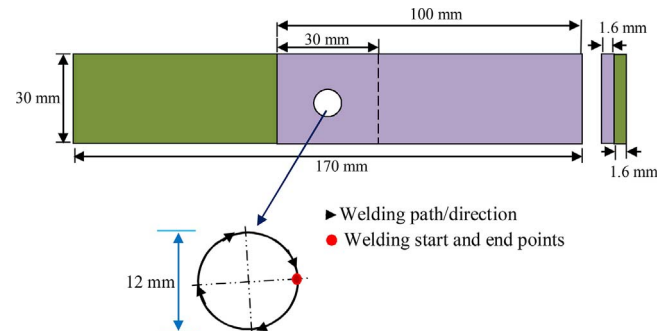


Fig. 1. Configuration of weld specimen and laser travel-path.

resultant surfaces of the weld specimen were etched in 2% tetrafluoroboric acid for 200 s and were subsequently rinsed with ethanol ( $\text{C}_2\text{H}_5\text{OH}$ ) after etching. The microstructure of the weld zones was viewed under ZEISS optical microscope. Likewise, Vickers microhardness values of the respective weld zones were determined by applying 500 g diamond indenter for 10 s across the cross section of welds.

## 3. Results and discussion

### 3.1. Microstructure

Figs. 4 a and 5 a show the macrographs of deep penetrated and partially penetrated welds of Alclad 2219-O aluminum alloy. Ring-like fusion zones are created in each of the weld categories and this implies that two-point bonded joint/fusion is only visible in the weld cross section as revealed in Figs. 4 a and 5 a respectively. Based on the manner in which the cross sections are obtained, these fusion regions are the start/end (S/E) fusion region and the travel-path (TP) fusion region respectively. The upper fusion width of S/E region in each weld is wider than that of the travel-path region and this is attributed to the effect of the returning laser beam on the weld during the keyhole welding process. Similarly, the fusion width of welds decreases along the penetration depth into the workpiece setup due to the dominant heat conduction effect (melting) or absorption of laser radiation by the molten metal at the weld surface region.

The fusion regions of the examined welds consist of porosity with different levels as revealed in Figs. 4 and 5. Fig. 4 shows a combination of micropores and coarse pores in the fusion regions of the start/end zone and that of the travel-path zone of the full penetrated weld. Mazar et al. (2016) reported that the sizes of macro-porosity and micro-porosity are within 300–600  $\mu\text{m}$  and 50–200  $\mu\text{m}$  respectively. The porosity sizes of the welds were studied. The macroporosity of the S/E region lies within 351–575  $\mu\text{m}$  while that of TP region lies between 304 and 450  $\mu\text{m}$ . These are in agreement with the examined literature values. Similarly, it is important to note that the full keyhole welding process is achieved at a higher laser power of about 3750 W and this is expected to induce higher vaporization and cause laser plume/metal vapor effects. As a result, the porosity levels of the full penetrated welds can be attributed to the vaporization of high vapor pressure elements in the AA2219 alloy. Likewise, according to Schneider et al. (2013), keyhole instabilities or intermittent closures of keyhole coupled with high welding speed and high rate of cooling significantly influence the formation of pores in laser weld. This could also have influenced the porosity of the full penetrated welds. In contrast to this, Chengcai and

**Table 2**  
Optical characteristics of the fibre laser.

Characteristics	Values
Operation mode	CW
Polarization	Random
Nominal output power, P <sub>nom</sub>	6000 W
Output power tuning range	10–105%
Emission wavelength	1070–1080 nm
Emission linewidth	3–6 nm
Switching on/off time	50–100 $\mu\text{s}$
Output power modulation rate	5 kHz
Output power instability	$\pm 1 - \pm 2\%$
Red guide laser power	0.4–0.5 mW

Download English Version:

<https://daneshyari.com/en/article/5017626>

Download Persian Version:

<https://daneshyari.com/article/5017626>

[Daneshyari.com](https://daneshyari.com)